nature electronics

Article

https://doi.org/10.1038/s41928-025-01407-0

Continuous biochemical profiling of the gastrointestinal tract using an integrated smart capsule

Received: 26 July 2024

Accepted: 27 May 2025

Published online: 27 June 2025

Check for updates

Jihong Min[1,6], Hyunah Ahn[1,2,6], Heather Lukas[1], Xiaotian Ma[1], Rinni Bhansali[1], Sung-Hyuk Sunwoo[1], Canran Wang[1], Yadong Xu[1], Dickson R. Yao[1], Gwangmook Kim[1], Zhaoping Li[3], Tzung K. Hsiai[4], Azita Emami[1,5], Hee-Tae Jung[2] ✉ & Wei Gao[1] ✉

The gastrointestinal tract contains a wealth of chemical information that can be used to decipher the health of the digestive and nervous systems. Traditional methods of analysis, such as faecal analysis and biopsies, are invasive, costly and incapable of providing real-time metabolic and hormone profiling across the gastrointestinal tract. Commercial ingestible capsule sensors have been developed, but only monitor basic markers, such as pH and pressure, neglecting detailed chemical analysis. Here we report an integrated smart capsule that can simultaneously detect a spectrum of biochemical markers, including electrolytes, metabolites and hormones. The capsule, which is termed PillTrek, is 7 mm in diameter and 25 mm in length, and houses a miniaturized wireless electrochemical workstation capable of executing a range of electrochemical measurement techniques (potentiometry, amperometry, voltammetry and impedimetry), allowing it to interface with a variety of electrochemical sensors and detect various parameters in the gut. Using an array of sensors (serotonin, glucose, pH, ionic strength and temperature), we illustrate the capabilities of the system in vitro and in vivo in animal studies involving rat and rabbit models, monitoring the dynamic profile of these crucial biomarkers and their responsiveness to different dietary intakes.

The gastrointestinal (GI) tract plays two key roles: as a conduit for nutrient absorption and waste expulsion, and as a complex interface linking overall health to internal physiological processes[1,2]. The system hosts the gut microbiota, which, alongside the central and enteric nervous systems, regulates a myriad of processes[3,4], including the breakdown and selective absorption of nutrients. It can also influence our emotional and cognitive states[5], directly through hormone production and indirectly by triggering brain signals through metabolites or stimulating immune cells to release cytokines[6,7]. Dysbiosis, a perturbation of the delicate ecosystem within the GI tract, is intertwined with a diverse array of disorders. These extend beyond GI issues (such as irritable bowel syndrome and inflammatory bowel disease) to central nervous system disorders (such as autism, anxiety, depression and Parkinson's disease)[8,9].

The biochemical profile of the GI tract governs its health and our overall well-being (Fig. 1a). For example, serotonin is crucial for regulating gut motility and substantially affects mood, appetite and cognitive functions, with about 95% of the body's serotonin synthesized in the GI tract[10,11]. Short-chain fatty acids, the end products of dietary fibre fermentation by anaerobic intestinal microbiota, play a role in maintaining gut health, regulating metabolism and supporting immune function[12,13]. The pH level in the GI tract affects digestive enzyme activity

A full list of affiliations appears at the end of the paper. ✉e-mail: heetae@kaist.ac.kr; weigao@caltech.edu

https://doi.org/10.1038/s41928-025-01407-0

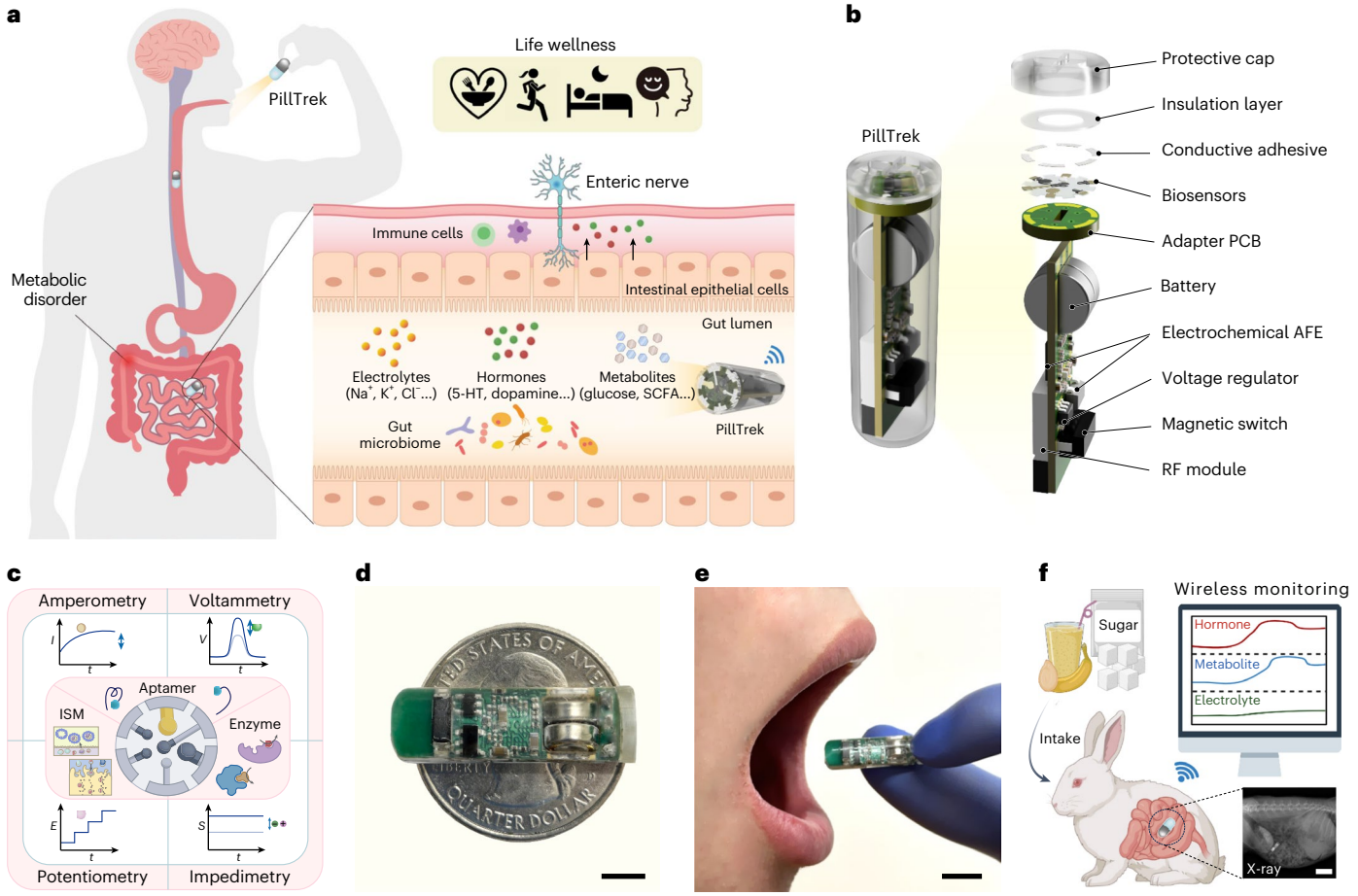

Fig. 1 | PillTrek, a capsule electrochemical platform for continuous, multiplexed GI fluid analysis. a, Illustration of the PillTrek navigating through the GI tract, flourishing with biochemical markers. 5-HT, serotonin; SCFA, short-chain fatty acid. **b**, Schematic of the fully assembled and exploded views of PillTrek, showing components including batteries, electronics, biosensors and protection. AFE, analogue front end; RF, radio frequency. **c**, Diagram demonstrating the various recognition elements compatible with PillTrek, such as ion-selective membranes (ISMs), aptamers and enzymes. The device supports diverse electrochemical techniques, including potentiometry, amperometry, voltammetry and impedimetry, for detecting a wide range of biochemical markers. *I*, current; *V*, voltage; *t*, time; *E*, potential; *S*, admittance. **d**,**e**, Photographs showcasing the miniature form factor (<1 cm^3) of the PillTrek, displayed on a coin (**d**) and held by a model (**e**). Scale bars, 0.5 and 1 cm, respectively. **f**, Schematic illustrating the miniaturized PillTrek monitoring diet-induced biomarker level changes in the intestines of a rabbit model. Scale bar, 3.5 cm. Schematic in **f** created with BioRender.com.

and the composition of gut microbiota, making it important for maintaining a healthy digestive system[14,15]. Ionic strength, which measures the concentration of ions in GI fluids, is essential for electrolyte balance and cellular function, with abnormalities potentially indicating various health issues[16]. Glucose levels provide information on nutrient absorption efficiency and metabolic health, influencing microbial activity in the gut and helping detect conditions like diabetes and malabsorption issues[17,18]. Monitoring GI biochemicals is thus essential for understanding metabolic health and functionality of the GI tract, and also for preventing and managing diseases[19,20].

Recent advances in wireless sensing technology have led to the development of ingestible capsules for GI tract monitoring[21–25]. Commercial ingestible technologies, such as capsule endoscopes and pH and/or pressure sensing capsules, primarily detect optical and physical alterations in the GI tract caused by underlying disorders[1,21]. While these devices aid in diagnosing disease symptoms, they frequently fail to reveal early signs or ascertain the underlying cause of the disease. Moreover, although emerging ingestible capsules have been used to monitor vital signs[26,27], gas molecules[28], radiotherapy[29] and inflammation[30,31], limitations persist in biomolecular profiling in the GI tract[32]. An ingestible capsule platform capable of continuously and selectively monitoring a broad spectrum of chemical signals in GI fluids could provide a more complete understanding of GI health, facilitating earlier diagnosis and intervention. However, development has been hindered by challenges related to selective in situ sensing, high variability in the GI environment and the integration of low-power miniaturized systems.

In this Article, we report an integrated smart capsule platform that encapsulates an electrochemical sensor array and a low-power wireless electronic system, and is capable of real-time, continuous and multiplexed monitoring of the GI tract (Fig. 1b). The platform, which we term PillTrek, has a compact form under 1 cm^3 in volume and is capable of monitoring a range of molecular biomarkers in complex gut fluids. It uses selective bioreceptors, including aptamers, enzymes and ion-selective membranes, to ensure precise target recognition. It can also perform a variety of signal transduction measurements, including potentiometry, amperometry, voltammetry and impedimetry, allowing it to interface with a range of electrochemical sensors and detect various parameters of interest in the gut (Fig. 1c–e). Compared to previously reported ingestible electronic capsules, PillTrek offers increased electrochemical sensing capabilities within a highly miniaturized form factor (Supplementary Table 1).

We develop and validate an array of GI biomarker sensors—including aptamer-based voltammetric serotonin sensors, enzymatic amperometric glucose sensors, ion-selective potentiometric pH sensors and impedimetric ionic strength sensors—for the analysis of GI biofluids,

such as intestinal fluids and faecal fluids. To achieve high-accuracy in situ sensing in the complex GI environment, various real-time calibration mechanisms are integrated, including an adaptive ratiometric dual-frequency measurement scheme for aptamer-based sensors, as well as pH, ionic strength and temperature compensation for the voltammetric and amperometric sensing. The fully integrated PillTrek is evaluated in vitro in the intestines of a rat model and in vivo in a rabbit model for the multiplexed analysis of GI biomarkers in response to nutrient-enriched diets (Fig. 1f). PillTrek has the potential to provide a nuanced biochemical portrait of the GI tract, revealing the intricate and often obscured chemical activities related to gut health and thereby facilitating the development of personalized monitoring and targeted therapies for safeguarding GI health.

PillTrek design for continuous biochemical monitoring

PillTrek consists of a rectangular main printed circuit board (PCB) (6.5×23 mm^2) for signal processing and wireless communication, and a circular adapter PCB (6.5 mm in diameter) that is mounted perpendicularly to the main PCB to directly interface the sensor array (Fig. 1b and Supplementary Figs. 1 and 2). The main PCB features a cavity to hold two silver oxide batteries (3.1 V, 16 mAh) that can be remotely disconnected from the circuit via a magnetic reed switch. This design allows the PCBs, once encapsulated in polydimethylsiloxane (PDMS) through injection moulding, to be stored next to a magnet for extended periods without draining the battery. During operation, the electronic system can maintain a Bluetooth Low Energy (BLE) connection and perform complex electrochemical analysis sequences continuously for more than 22 h.

Meanwhile, the sensor array is mass-produced sequentially through laser patterning to form vias for contacting the adapter PCB and through inkjet printing to accurately pattern gold, carbon and silver electrodes (Supplementary Fig. 1). After sensor modification, the sensor array is patterned and conductively affixed to the encapsulated electronic system. Additionally, the array is then protected by a three-dimensionally printed chamber, creating a fully packaged capsule system with a diameter of 7 mm and a length of 25 mm. This size is comparable to common pills and substantially smaller than most electronic capsule systems on the market or reported in the literature (Fig. 1g,h, Supplementary Figs. 2 and 3 and Supplementary Table 2).

Multiplexed sensor array for GI biomarker detection

A custom-developed miniaturized sensor array was designed for real-time, multimodal monitoring of four distinct biomarkers in GI fluids. Integrated with a versatile electronic system, this sensor array can multiplex amperometric, impedimetric, potentiometric and voltammetric techniques to interface a wide spectrum of sensors that incorporate recognition elements such as enzymes, ion-selective membranes and aptamers. For this study, we selected an array of gut biomarkers, including the hormone serotonin, the metabolite glucose, pH and ionic strength (Fig. 2a). The sensor array is constructed on a polyethylene terephthalate (PET) substrate with mass-producible inkjet-printed electrodes, ensuring both adaptability and precision in detection processes (Fig. 2b). The modified electrode array, mounted on the capsule electronic system, can accurately detect a wide range of key biomarkers in GI fluids, including serotonin, glucose, pH and ionic strength (Fig. 2c–e).

Each sensor within the array has been meticulously optimized for robust detection in GI fluids. For the selective detection of intestinal glucose levels, glucose oxidase (GOx) was immobilized in a highly permeable and biocompatible chitosan matrix atop a Prussian blue redox mediator layer to facilitate electron transfer from GOx to the electrode. Given that Prussian blue exhibits poor stability in biofluids due to gradual degradation in neutral and alkaline solutions, a protective thin layer of the Prussian blue-analogue nickel hexacyanoferrate (NiHCF) was deposited on Prussian blue to enhance the glucose sensor's durability[33]. To accommodate the wide range of physiologically relevant glucose levels in the GI tract, a polyurethane diffusion-limiting layer was coated on the glucose sensor. This layer acts as a semipermeable membrane, controlling glucose diffusion to the enzyme layer and effectively extending the sensor's linear range by preventing rapid saturation of GOx (Supplementary Fig. 4)[34]. The glucose sensor exhibits a consistent linear response to glucose concentrations ranging from 0 to 50 mM with a sensitivity of −2.78 nA mM^{-1} (Fig. 2f). The pH sensor features an electrodeposited polyaniline (PANI) layer as an ion-selective membrane and shows a consistent linear response from pH 4 to 8 with a sensitivity of 54.84 mV per pH (Fig. 2g). To quantify the ionic strength of target solutions, impedance is measured between two carbon electrodes. The ionic strength sensor accurately measures salt concentrations from 0.1× to 2× simulated intestinal fluid (SIF) with a sensitivity of 7.15 mS mM^{-1}, with 1× SIF approximating 140 mM (Fig. 2h). These sensors are capable of automatic regeneration for up to ten iterations, allowing for continuous biomarker monitoring (Supplementary Fig. 5).

In situ detection of serotonin in the gut fluid is highly challenging due to its low concentration, the complex fluid matrix and the presence of major interfering electroactive molecules. Traditional oxidation-charge detection approaches, based on fast-scan cyclic voltammetry or differential pulse voltammetry, offer high temporal resolution and sensitivity but fail to selectively monitor basal serotonin levels in gut fluids[35,36]. To achieve both sensitivity and selectivity for serotonin detection, an inkjet-printed AuNP (gold nanoparticle) electrode with a large electroactive surface area (~0.1113 cm^2) was integrated with a serotonin aptamer tagged with the redox molecule methylene blue (Supplementary Fig. 6). When the aptamer binds to the serotonin molecule, target binding-induced conformational changes alter the distance of the methylene blue redox reporter from the electrode surface, resulting in varied electron transfer efficiency. Nuanced and reversible detection of varying serotonin concentrations can be achieved by quantifying the methylene blue redox signal via square wave voltammetry (SWV). Depending on the SWV frequency, the SWV peak currents decrease or increase (signal-off or signal-on) or remain constant regardless of analyte concentration (non-responsive) due to the binding dynamics of the aptamer probe (Supplementary Fig. 7). The serotonin aptamer sensor could demonstrate log-linear responses between physiologically relevant serotonin levels (0 to 100 μM) (Fig. 2i,j). Additionally, a slight negative shift in the SWV peak potential was observed with increasing serotonin concentration due to conformational changes in the aptamer affecting electron transfer kinetics of the methylene blue probe[37]. The aptamer conditions for aptamer functionalization, such as concentration and incubation time, were optimized to achieve a high SWV peak current height and equilibrium aptamer–serotonin reaction, thereby enhancing sensitivity (Supplementary Figs. 8 and 9).

To mitigate the influence of sensor-to-sensor variations and the complex biofluid matrix to sensing accuracy of the aptamer-based serotonin sensor, a dual-frequency method is used (Supplementary Note 1). In this approach, the signal-off or signal-on frequency response is calibrated against the non-responsive frequency response where the sensor response is independent of analyte concentration as the bound and unbound state currents are equal[38]. To maximize sensor performance in SIF, we identified the optimal SWV parameters as follows: responsive frequency of 10 Hz, non-responsive frequency of 20 Hz and amplitude of 45 mV (Supplementary Figs. 10 and 11). With optimized parameters, we were able to achieve a low detection limit of 50 nM and a log-linear sensor response over a wide range of serotonin levels with a sensitivity of −0.0071 μM^{-1} in SIF using this dual-frequency method (Fig. 2j). Additionally, the serotonin sensor can be automatically and readily regenerated in SIF as serotonin levels change, indicating its

https://doi.org/10.1038/s41928-025-01407-0

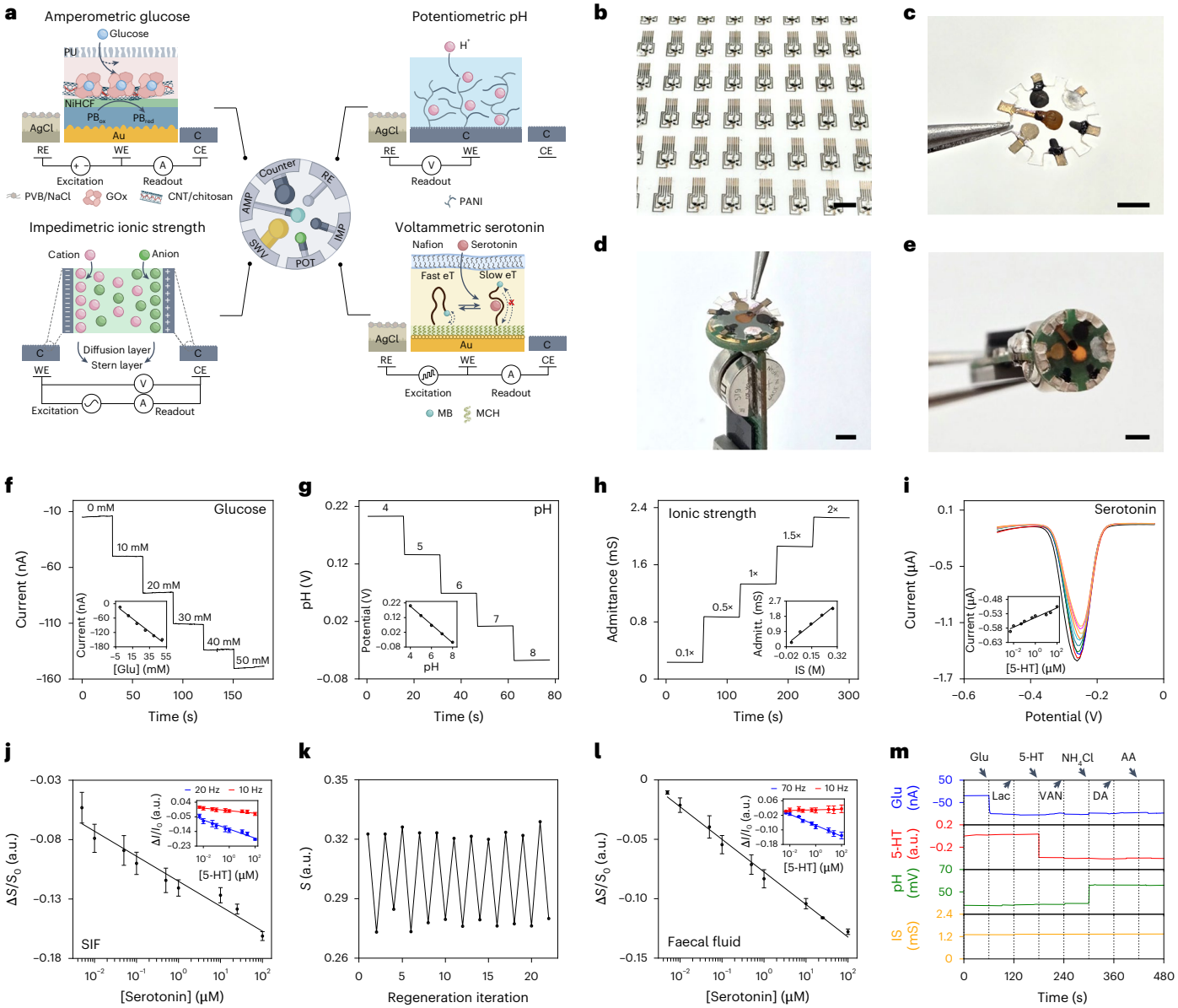

Fig. 2 | Electrochemical sensor array of PillTrek for multiplexed detection of GI biomarkers. a, Schematic of inkjet-printed electrochemical sensor array, detailing the operation mechanism of four integrated sensors: amperometric enzyme-based glucose sensor, potentiometric ion-selective pH sensor, impedimetric ionic strength sensor and voltammetric aptamer-based serotonin sensor. PU, polyurethane; CNT, carbon nanotube; RE, reference electrode; WE, working electrode; CE, counter electrode; MB, methylene blue; eT, electron transfer; MCH, mercaptohexanol; AgCl, silver chloride; NaCl, sodium chloride; POT, potentiometry; IMP, impedimetry; AMP, amperometry; H^+, hydrogen ion. **b**, Photograph of inkjet-printed sensor array on a PET substrate. Scale bar, 1 cm. **c**–**e**, Photographs of a standalone biosensor array (**c**) and a biosensor array before (**d**) and after (**e**) integration into the capsule system. Scale bars, 0.2 cm. **f**–**i**, Electrochemical responses of each sensor. **f**, Amperometric glucose. **g**, Potentiometric pH. **h**, Impedimetric ionic strength (IS). **i**, SWV response of the serotonin sensors at a signal-off SWV frequency of 10 Hz. Black lines in **f**–**i** insets indicate linear-fit trendlines. Insets in **f**–**i** represent the corresponding calibration plot of each sensor. **j**, Calibration curve based on the relative ratiometric signal ($S = I_{10Hz}/I_{20Hz}$) of the serotonin sensor in SIF, where I is the SWV peak current height. The inset shows relative changes in peak current under 10 and 20 Hz. Black, red and blue lines indicate linear-fit trendlines. S_0 and I_0 indicate relative ratiometric signal and SWV peak current height at blank serotonin concentration, respectively. Error bars represent the s.d. of the mean from three sensors. **k**, Continuous sensing and regeneration of the serotonin sensor in SIF containing 0.1 and 10 μM serotonin. **l**, Calibration curve of the serotonin sensor in human faecal fluid ($S = I_{10Hz}/I_{70Hz}$). Black, red and blue lines indicate linear-fit trendlines. Error bars represent the s.d. of the mean from three sensors. **m**, Selectivity test of the sensor array in SIF on the sequential addition of 10 mM glucose (Glu), 10 mM lactate (Lac), 20 μM serotonin (5-HT), 20 μM vancomycin (VAN), 10 mM ammonium chloride (NH_4Cl), 20 μM dopamine (DA) and 20 μM ascorbic acid (AA).

capability for continuous target monitoring (Fig. 2k). Furthermore, these aptamer-based sensors demonstrated batch-to-batch reproducibility and high stability over a 15-day storage period at 4 °C (Supplementary Fig. 12). To further enhance the sensor performance in biofluids, a 0.5%-Nafion anti-fouling protective layer was applied, which facilitates the exclusion of large molecules and provides electrostatic repulsion through a negatively charged polymer network (Supplementary Figs. 13 and 14)[39,40].

The developed glucose, pH and serotonin biosensors were successfully evaluated in real biofluids for target biomarker analysis. In human serum, human faecal fluid and intestinal fluids collected from rats and rabbits, all biosensors demonstrated stable linear or log-linear

https://doi.org/10.1038/s41928-025-01407-0

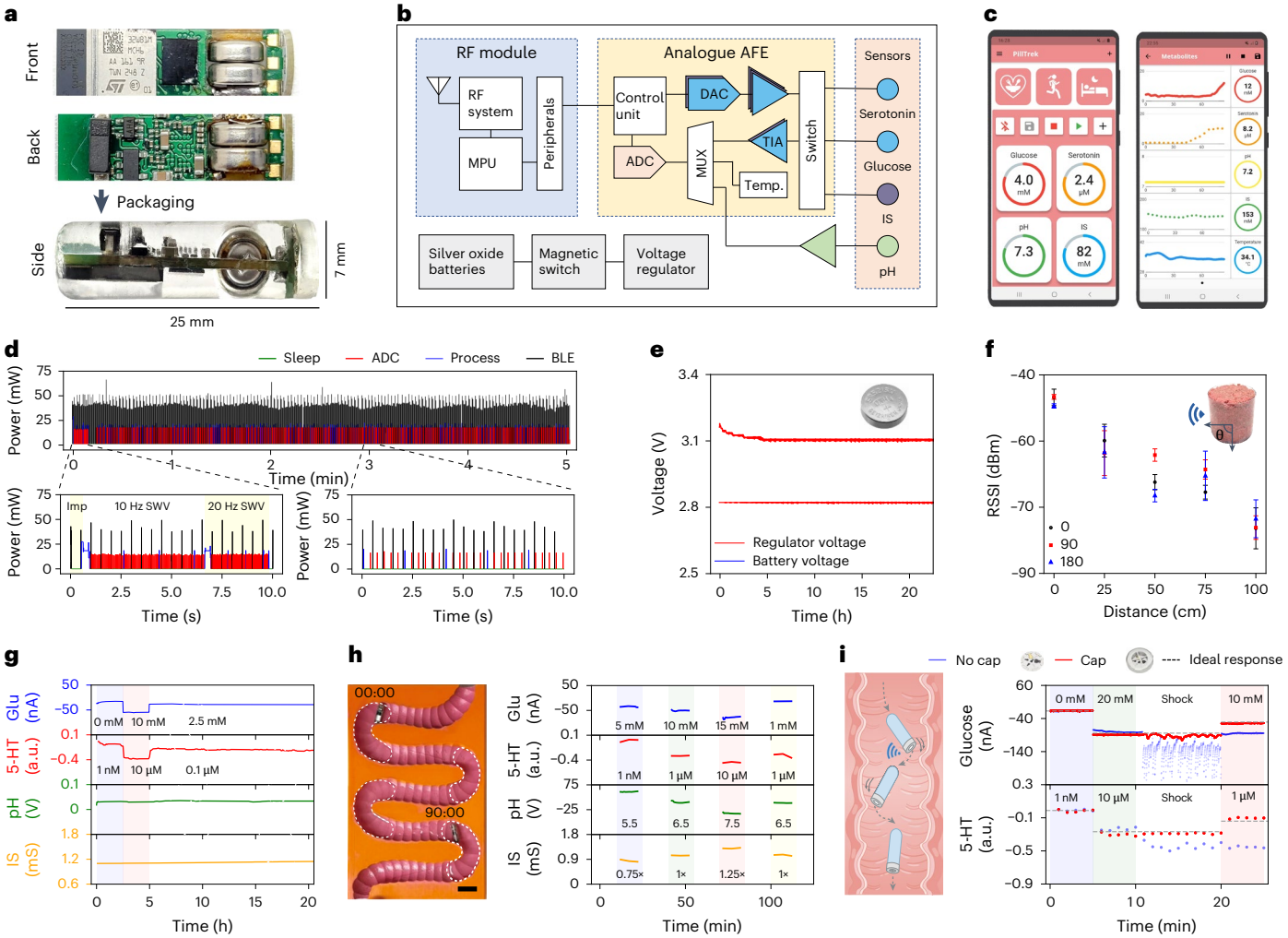

Fig. 3 | The system integration of PillTrek for prolonged wireless operation in the GI tract. a, Photographs of the electronic system from the front view (top) and back view (bottom) before PDMS encapsulation, and side view of the fully packaged device. **b**, System-level block diagram of PillTrek. RF, radio frequency; MPU, microprocessor unit; ADC, analogue to digital converter; DAC, digital to analogue converter; MUX, multiplexer; TIA, transimpedance amplifier; Temp., temperature. **c**, Custom mobile application for monitoring data from PillTrek. **d**, Real-time power consumption profile of PillTrek during continuous multimodal sensing operation over a 5-min repeated cycle (top), with zoomed-in power profiles during impedance, SWV (bottom left) and multiplexed amperometric, potentiometric and temperature measurements (bottom right). Imp, impedance. **e**, Long-term battery performance and voltage regulator output potential during continuous multimodal sensing operation. **f**, The receiver signal strength intensity (RSSI) of PillTrek when placed in a meal-filled container, measured by a smartphone from varying angles up to 1 metre away. Error bars represent the s.d. of the mean from multiple measurements ($n = 20$). **g**, Long-term operation and multimodal sensing stability of PillTrek in SIF, showing electrochemical responses of glucose, serotonin, pH and ionic strength sensors. nA, nanoampere. **h**, Dynamic biomarker tracking capability of PillTrek as it travels through a phantom intestine model over a 90-min period. Scale bar, 2.5 cm. **i**, Glucose (top) and serotonin (bottom) sensor responses of PillTrek devices with and without a protective cap, demonstrating the impact of repeated contact with intestinal tissue.

sensor response and low sensor-to-sensor variations across the physiologically relevant biomarker concentration ranges (Fig. 2l, Supplementary Figs. 15–18 and Supplementary Table 3). To maintain desired functionality in biofluids, the current sensor configuration is designed for operation in the small and large intestines, which exhibit a typical pH range of 6.5 to 8. It should be noted that while the serotonin sensor maintained its original signal-off responsive frequency of 10 Hz, the non-responsive frequencies varied in different sample matrices: 30, 50, 70 and 70 Hz were identified as the non-responsive frequencies for PBS, serum, faecal fluid and intestinal fluids (Supplementary Fig. 19). Furthermore, while the serotonin sensor's bare SWV peak current is subject to sensor-to-sensor variations that universally affect aptamer-based sensors[38], the use of a ratiometric signal (S) between the peak currents at responsive and non-responsive frequencies improves reproducibility (Supplementary Fig. 20). The accuracy of the serotonin sensors for biofluid analysis was validated using the laboratory gold-standard enzyme-linked immunosorbent assay (ELISA) with rat intestinal fluids, resulting in a linear correlation coefficient of 0.91 between the ELISA and biosensor measurements (Supplementary Fig. 21).

When integrated into the multiplexed sensor patch, all sensors display high selectivity against common interferent molecules such as glucose, lactate, dopamine, vancomycin, ammonium chloride and ascorbic acid (Fig. 2m). Given that the sensor may encounter diverse environments, including sludge-like substances in the GI tract, we validated its consistent performance in both liquid (SIF) and solid (2% agarose hydrogel presoaked in SIF for 2 h) media (Supplementary Fig. 22). Additionally, the sensor array's dependence on factors such as solution pH, ionic strength and temperature was thoroughly studied to ensure reliable operation in the dynamic environment of the intestines, a key site of metabolic and hormonal activities (Supplementary Figs. 23–28). The glucose, serotonin and ionic strength sensors showed increased responses with rising temperatures. The serotonin sensor was also

found to be sensitive to changes in solution pH and ionic strength, while maintaining its selectivity against other catecholamines within the pH range typically found in the intestine (Supplementary Fig. 27). Furthermore, temperature variations affected the electron transfer kinetics of the serotonin sensor, resulting in different non-responsive frequencies. By incorporating real-time sensor calibration based on fluid pH, ionic strength and temperature, accurate in situ gut fluid biomarker analysis can be achieved (Supplementary Note 2).

System-level integration of capsule electronic device

In the creation of a capsule electronic system, paramount considerations were directed towards its size, power efficiency and wireless transmission capabilities to facilitate accurate measurements within the GI tract. Emphasizing miniaturization, PillTrek features a compact form factor, occupying a volume just under 1 cm^3, ensuring high ingestibility and easy manoeuvrability through the GI transit pathways (Fig. 3a). At its core, the main PCB integrates essential components such as silver oxide batteries, a magnetic reed switch and a low drop-out voltage regulator for stable power delivery to the wireless sensor interface (Fig. 3b, Supplementary Fig. 29 and Supplementary Table 4). To provide a stable supply voltage to the analogue circuitry, the 3.1 V battery voltage is regulated to 2.8 V for powering the radio frequency module and electrochemical analogue front end. This wireless sensor interface supports a comprehensive suite of electrochemical techniques, including potentiometry, amperometry, SWV and impedance measurements with data wirelessly transmitted to a custom mobile phone application (Fig. 3c).

Power management is a crucial facet of the design strategy, aimed at promoting operational stability and longevity. To optimize power consumption during multimodal operation, a custom-developed embedded algorithm keeps the electronic system in sleep mode for most of the time, waking it briefly for transient data measurement, processing and transmission events (Supplementary Fig. 30). The system operates on a 5-min cycle, performing an impedimetric measurement followed by two SWV scans at responsive and non-responsive frequencies in the first 10 s, and then multiplexed potentiometric, amperometric and temperature measurements for the remainder of the cycle, resulting in an average power consumption below 350 μW (Fig. 3d, Supplementary Fig. 31 and Supplementary Table 5). Powered by two silver oxide batteries in series, the PillTrek system, while performing continuous multimodal measurements, can maintain a stable supply voltage of 2.8 V for over 20 h (Fig. 3e).

Furthermore, wireless data transmission capabilities are critical for enabling real-time monitoring of GI biomarkers in vivo. To evaluate the wireless signal strength through tissue, the capsule, intended for testing in a rabbit model, was placed in the centre of a cylindrical tank (12-inch diameter, 12-inch height) filled with ground pork (Fig. 3f). The receiver signal strength intensity was measured at various angles relative to the capsule's orientation within the tank. Signal strengths higher than −90 dBm were recorded up to a metre away from the cylindrical tank, demonstrating the system's ability to reliably transmit data through dense biological tissue. Additionally, the capsule system was fully sealed, with no change in weight observed over 24 h in rabbit intestinal fluid and the electronic system remained fully functional afterwards (Supplementary Fig. 32).

The long-term multiplexed sensing capability of the capsule was validated by submerging the device in an intestine-simulating tube filled with SIF, exposing it to dynamic glucose and serotonin concentrations for over 20 h (Fig. 3g and Supplementary Video 1). This further confirmed the system's ability for continuous operation, the robust integrity of its encapsulation and the long-term stability of the electrochemical sensors. To simulate in vivo conditions with continuous motion and intermittent fluid availability, the capsule system was pulled through a phantom intestine with SIF-filled wells for 2.5 h using a stepper motor, reel and string (Fig. 3h and Supplementary Figs. 33 and 34).

To mitigate the influence of mechanical contact on sensor performance, a three-dimensionally printed cap was added to the sensor array. Two capsule devices, one with and one without the protective cap, underwent controlled and repetitive collisions for 10 min. The sensor responses following the collisions were recorded (Fig. 3i, Supplementary Video 2 and Supplementary Fig. 35). The capped sensors maintained stable responses during the test, while uncapped sensors experienced altered responses with only the pH and ionic strength sensors recovering functional responses afterward.

As PillTrek is designed for internal use in the GI tract, its biocompatibility is crucial for practical applications. The cell viability of cells seeded on a PillTrek was analysed using a commercial live–dead kit. Live–dead staining images of human colorectal adenocarcinoma HT29 cells over extended culture periods demonstrated robust cell viability (Supplementary Fig. 36). This underscores the high cytocompatibility of PillTrek, supporting its potential use for in vivo tests.

In vitro evaluation of PillTrek for dietary response

While the blood biomarker levels postdietary intake are well studied, GI biomarker levels remain obscure due to the inaccessibility of these fluids. However, understanding biochemical profile of intestinal fluids can elucidate the complex interplay of various GI physiologies. Given the well-documented influence of diet on the human gut microbiome[41], the multimodal capsule sensor array was first used for the in vitro evaluation of GI biomarker levels in response to varying dietary intakes.

After fasting for 12 hours, three groups of rats were further fasted, given 1 M sugar-infused water or given a tryptophan-rich smoothie for an additional 2 hours. The intestines of the euthanized rats were sectioned into five segments, and the intestinal fluids were harvested and analysed with the PillTrek sensor platform (Fig. 4a–h). Rats that drank sugar water had visibly bloated intestines, probably due to the osmotic effects of the high sugar concentration (Fig. 4a and Supplementary Fig. 37).

Fasting rats had low glucose concentrations (<3 mM) throughout the GI tract, with serotonin levels of 4.06 ± 1.55 μM in the small intestine and 5.53 ± 3.31 μM in the large intestine (Fig. 4b,e,f). The larger variation in serotonin measurements in the large intestine may be attributed to its more heterogeneous environment. Rats exposed to sugar water consumed 9–10 g, resulting in high glucose levels in the small intestine (40.5 ± 7.49 mM) and moderately elevated levels in the large intestine (10.5 ± 6.70 mM) (Fig. 4c,e). Serotonin levels in the small and large intestines were lower than in fasted animals, at 3.24 ± 1.26 and 4.13 ± 1.61 μM, respectively (Fig. 4f). This decrease may be due to high glucose concentrations downregulating tryptophan hydroxylase expression or altering metabolic pathways and receptors, thereby reducing serotonin production and release from enterochromaffin cells[42,43].

The last group of rats consumed 6–8 g of a high tryptophan smoothie containing ingredients such as bananas and chia seeds (Fig. 4d). Glucose concentrations in these rats were elevated, although less than those in the sugar water group, at 19.2 ± 9.31 mM in the small intestine and 4.12 ± 0.78 mM in the large intestine, respectively (Fig. 4e). Serotonin levels in the small and large intestines were substantially higher, at 8.07 ± 3.03 and 11.1 ± 2.52 μM, respectively (Fig. 4f). This increase could be attributed to the high tryptophan content in the smoothie, promoting serotonin production by enterochromaffin cells through the tryptophan hydroxylase and aromatic amino acid decarboxylase pathway. Elevated serotonin levels in the colon, where the smoothie probably had not reached within 2 h, suggest additional factors at play[44].

The pH of the intestinal fluids was consistent across all rats, while ionic strength was highest in fasted rats (Fig. 4g,h). Intra-animal trends were also noticeable: glucose levels were consistently higher in the small intestine compared to the large intestine, probably due

https://doi.org/10.1038/s41928-025-01407-0

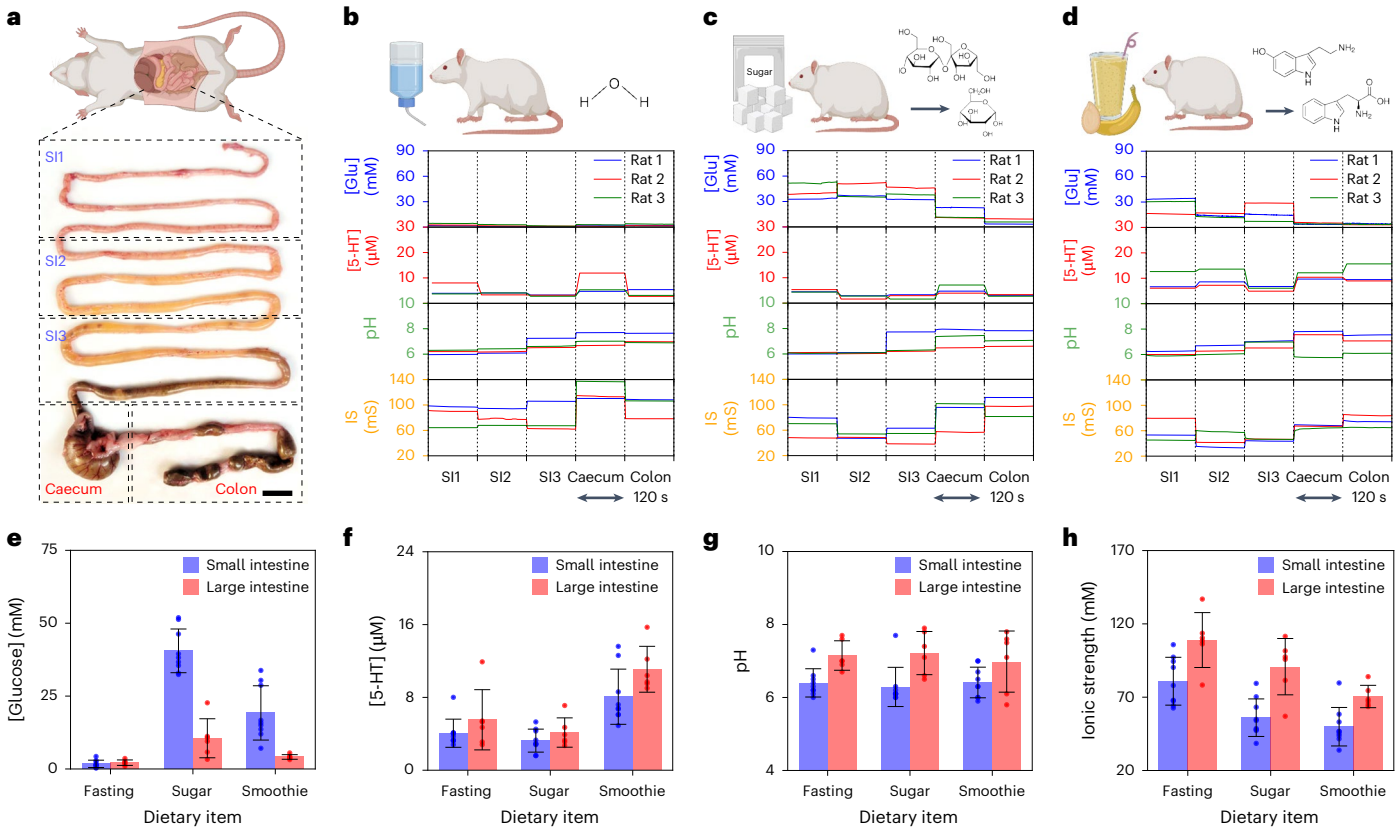

Fig. 4 | In vitro evaluation of PillTrek for assessing the dietary influences on GI biomarker levels in rats. a, Intestines of a rat divided into five sections for regional analysis. SI, small intestine. Scale bar, 1 cm. **b**–**d**, Glucose, serotonin, pH and ionic strength levels in various intestinal sections of fasted rats (**b**), rats after sugar water intake (**c**) and rats after tryptophan-rich smoothie intake (**d**) measured with the biosensor array. **e**–**h**, Bar plots representing the levels of glucose (**e**), serotonin (**f**), pH (**g**) and ionic strength (**h**) in the small (SI1, SI2 and SI3) and large (caecum and colon) intestines of rats after different dietary intakes. Error bars represent the s.d. of the mean from intestine samples ($n = 9$ for small intestine, $n = 6$ for large intestine). Illustrations in **a**–**d** created with BioRender.com.

to the rapid glucose absorption in the small intestine. Conversely, the serotonin levels were generally greater in the large intestine, where enterochromaffin cells are more abundant and short-chain fatty acids from carbohydrate fermentation by gut microbiota stimulate serotonin release[6]. Higher pH and ionic strength levels in the large intestine can be attributed to the production of alkaline substances by gut microbiota and the reabsorption of water and electrolytes, concentrating ions in the intestinal fluid. The receiver operating characteristic curves demonstrated PillTrek's ability to distinguish between fasted and smoothie-fed rats, with an area under the curve greater than 0.89 for the glucose, serotonin and ionic strength sensors (Supplementary Fig. 38)

In vivo real-time GI profiling in rabbits using PillTrek

The miniaturized capsule is compact enough to easily navigate through the small intestine of a rabbit (diameter of duodenum 1.71 ± 0.11 cm)[45]. To demonstrate PillTrek's capability for real-time in vivo monitoring of biomarkers, rabbits were fasted for 12 h before the surgical insertion of the capsule and a duodenostomy tube into the duodenum, a key site for nutrient absorption and hormonal signalling. Serotonin and glucose levels in the GI tract were modulated through a peristaltic pump, altering biomarker levels, while the capsule device performed multiplexed measurements and wirelessly transmitted data on intestinal glucose, serotonin, pH, ionic strength and temperature levels (Fig. 5a and Supplementary Fig. 39).

During the procedure, the rabbits' vital signs were continuously monitored to ensure their health, and X-ray images confirmed the PillTrek's location and locomotion within each rabbit's GI tract (Fig. 5b,c and Supplementary Fig. 40). Throughout the study in two different rabbits, the capsule systems accurately monitored changes in biomarker concentrations. A continuous infusion of 10 μM serotonin was administered at 30 min, followed by an infusion of 20 mM glucose in addition to the 10 μM serotonin at 60 min. The sensor responses were calibrated in real time based on temperature, pH and ionic strength (Supplementary Note 2). PillTrek accurately monitored the trends in which measured serotonin and glucose levels gradually increased after 30 and 60 min, respectively, following nutrient delivery, and remained stable over time. Consistent GI pH, temperature and ionic strength were observed throughout the study. In a follow-up in vivo rabbit study, the capsule accurately monitored dynamic changes in serotonin levels as we administered a continuous infusion of 10 μM serotonin at 30 min, followed by blank saline at 60 min, thereby demonstrating the in vivo regeneration capability of the serotonin sensor (Supplementary Fig. 41).

Conclusions

PillTrek overcomes the limitations of traditional invasive methods and existing commercial capsule devices by providing simultaneous, continuous and multiplexed monitoring of key biochemical markers (such as pH, glucose, serotonin, ionic strength and temperature) in complex GI environment, offering detailed chemical profiles non-invasively. It has the potential for widespread adoption in continuous GI health monitoring. By providing real-time insights into the GI tract's biochemical environment, it could enhance our ability to explore and monitor the effects of various interventions on GI health. Future directions

https://doi.org/10.1038/s41928-025-01407-0

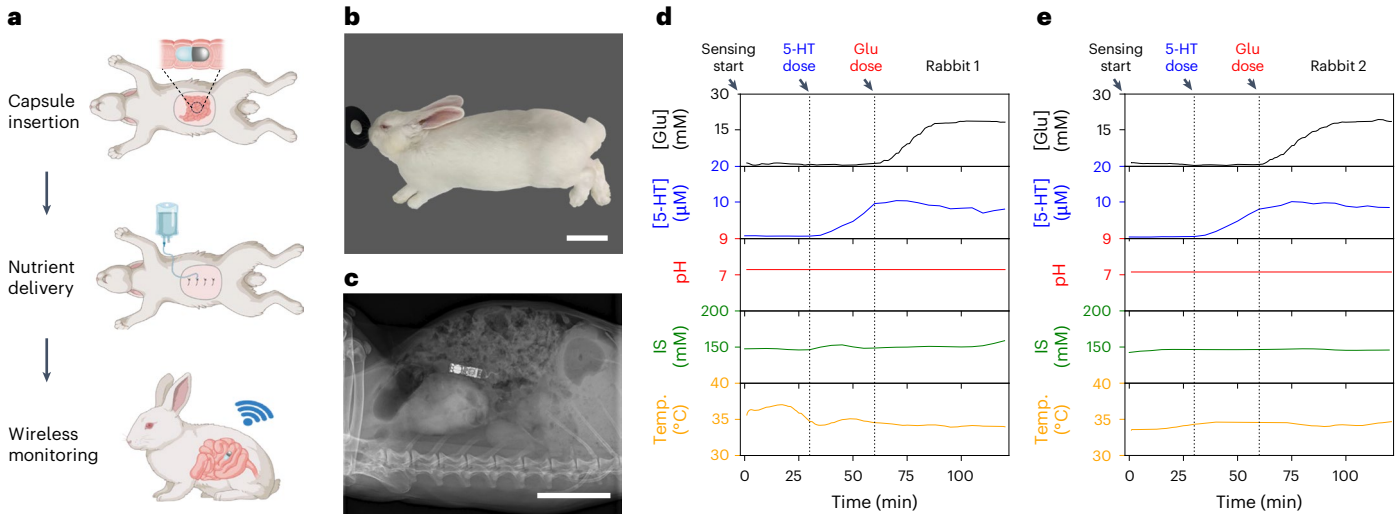

Fig. 5 | In vivo validation of PillTrek for real-time multimodal monitoring of GI biomarkers in rabbits. a, Schematic illustrating the experimental flow for in vivo rabbit studies. **b**, Photograph of the sutured stomach of a rabbit during the in vivo study. Scale bar, 10 cm. **c**, X-ray image showing the location of PillTrek in the rabbit intestines. Scale bar, 5 cm. **d**,**e**, PillTrek-enabled multimodal GI biomarker profiling in rabbit 1 (**d**) and in rabbit 2 (**e**). Illustrations in **a** created with BioRender.com.

include expanding the range of detectable biomarkers and refining the technology for human clinical applications, paving the way for personalized GI health monitoring. Additionally, future studies will investigate how different long-term dietary interventions affect GI biomarkers, potentially linking these changes to behavioural outcomes and deepening our understanding of the gut–brain axis. Ultimately, this multidimensional approach has the potential to link gut biochemical dynamics with observable behavioural manifestations, enhancing our understanding of GI health and assisting in the development of personalized and precision medicine in both GI and central nervous system health.

Methods

Materials and reagents

Silver nitrate, iron chloride(III) and hydrogen tetrachloroaurate(III) hydrate were purchased from Alfa Aesar. Mercaptohexanol, sodium thiosulfate pentahydrate, sodium thiosulfate pentahydrate, polyvinyl butyral (PVB) resin BUTVAR B-98, tris(hydroxymethyl)aminomethane hydrochloride (Tris-HCl), tris-(2-carboxyethyl)-phosphine hydrochloride (TCEP), EDTA, Nafion 117, L-lactic acid, hydrochloric acid and toluene were purchased from Sigma Aldrich. Potassium ferric yanide(III) and potassium ferrocyanide(IV) was purchased from Acros Organics. Potassium chloride, *N*,*N*-dimethylformamide, D-glucose anhydrous and serotonin hydrochloride were purchased from Thermo Fisher Scientific. Sodium chloride, dimethylformamide, calcium chloride dihydrate, 10× PBS, magnesium chloride and acetic acid were purchased from Fisher Scientific. The ELISA kit for serotonin analysis was purchased from DLD Diagnostika GmbH. PET films (75 μm thick) were purchased from McMaster-Carr. The serotonin aptamer 5′-Thiol-C_6Linker-CGACTGGTAGGCAGATAGGGGAAGCTGATTCGATGCGTGGGTCG-MB-3′ was ordered from Integrated DNA Technologies. Carbon ink (5 wt%) and silver ink (25 wt%) were purchased from NovaCentrix. Gold ink (10 wt%) was purchased from C-INK Co. Ltd. PDMS (SYLGARD 184) was purchased from Dow Corning. Serum was purchased from the American Type Culture Collection (ATCC). Plain Au electrodes (as the control) were fabricated on a PET substrate by photolithography and electron-beam evaporation (30 nm Cr/100 nm Au).

Assembly of the capsule device

A two-part aluminium mould for the capsule device, consisting of a cylindrical cavity for device encapsulation and lid for device alignment, was fabricated by milling an aluminium block as designed by Fusion 360. Meanwhile, the main PCB was milled to form a cavity that fits two silver oxide batteries, and nickel tabs were soldered on the inner walls of the PCB cavities for holding and forming an electrical contact with the batteries. A slight extrusion in the main PCB was used as a plug to align and fit into the slot of the adapter PCB, before soldering the connection pads (Supplementary Fig. 1). After assembling the PCBs and batteries, the electronic system was fixed on the aluminium mould lid and then submerged into the PDMS filled aluminium cavity mould. A magnet was attached to the mould during PDMS curing to prevent battery discharge through a PCB mounted magnetic reed switch. After PDMS encapsulation, the sensor array prepared as described in the section below was conductively glued onto the adapter PCB using silver paint, before fixing a protective cap fabricated by a resin three-dimensional (3D) printer (ELEGOO Mars 3).

Preparation and characterization of the multimodal sensory array

A 50-W CO_2 laser cutter (Universal Laser System) was used to pattern vias on a PET substrate, creating electrical contacts between the sensor array and adapter PCB before inkjet printing the electrode arrays. The substrates were then cleaned by O_2 plasma surface treatment (Plasma Etch PE-25, 10–20 cm^3 min^{-1} O_2, 100 W, 150–200 mTorr) to remove debris and enhance surface hydrophilicity. An inkjet printer (DMP-2850, Fujifilm) was used to print gold, carbon and silver electrodes for the multimodal sensors, as well as SU-8 for electrode insulation. Specifically, the glucose, serotonin, pH and ionic strength sensors had diameters of 1, 1.2 and 0.4 mm, respectively. Furthermore, the reference and counter electrodes had diameters of 0.5 and 1.2 mm, respectively. The reference and working electrodes were further modified via electrochemical deposition (CHI 660E) and drop-casting methods. Both the electrochemical workstation and a capsule device were applied in the sensor characterization procedures.

Serotonin sensor. Aptamers were prepared by dissolving them to a concentration of 100 μM in 1× Tris-EDTA buffer, and then frozen in individual aliquots at −20 °C. The AuNP electrode was electrochemically cleaned using cyclic voltammetry in 0.5 M NaOH, executing 100 cycles from −1 to −1.6 V at a scan rate of 1 V s^{-1}, and subsequently rinsed with deionized water. Concurrently, TCEP reduction was carried out to reduce disulfide bonds by mixing 5 μl of a 10 μM DNA aliquot and

5 µl of 1 mM TCEP at room temperature in the dark for 1 h, followed by dilution with 1× PBS (pH 7.4) to 2.5 µM. The aptamer (2.5 µM, 5 µl) was immobilized onto the cleaned working electrode by incubation for 2 h at room temperature in the dark, and unbound aptamers were rinsed with 1× PBS. Overnight, 5 mM mercaptohexanol in 1× PBS was used to passivate the unbound electroactive surface of the Au electrodes, and finally the aptamer-modified electrodes were thoroughly rinsed with 1× PBS. For measurements in real biofluids, 0.5% Nafion was drop-casted and incubated overnight. The Nafion-modified sensors were rinsed with 1× PBS.

Glucose sensor. A nanostructured Au film was electrodeposited on the carbon electrodes to increase the electrode surface area, involving multipotential deposition in a solution of 50 mM chloroauric acid and 0.1 M HCl, undergoing 1,500 cycles (−0.9 V for 0.02 s and 0.9 V for 0.02 s). The Prussian blue (PB) layer was deposited onto the nanostructured Au electrodes in a fresh solution containing 2.5 mM $FeCl_3$, 2.5 mM $K_3[Fe(CN)_6]$, 100 mM KCl and 100 mM HCl by 20 cyclic voltammetry cycles (−0.2 to 0.6 V versus Ag/AgCl) at a scan rate of 50 mV s^{-1}. The NiHCF layer was then deposited in a fresh solution containing 0.5 mM $NiCl_2$, 0.5 mM $K_3Fe(CN)_6$, 100 mM KCl and 100 mM HCl by 25 cyclic voltammetry cycles (0 to 0.8 V versus Ag/AgCl) at a scan rate of 100 mV s^{-1}. For an enzyme solution, 1% chitosan was dissolved in a 2% acetic acid by magnetic stirring for 1 h, followed by mixing with 2 mg ml^{-1} multiwall carbon nanotubes through ultrasonication. GOx (10 mg ml^{-1} in 1× PBS) was mixed with chitosan and multiwall carbon nanotube solution with a volume ratio of 2:1. Next, 1 µl of enzyme cocktail was drop-casted onto the NiHCF/PB/carbon electrode and dried. Finally, 2 µl of polyurethane solution containing 15 mg ml^{-1} polyurethane in tetrahydrofuran and *N*,*N*′-dimethylformamide (volume ratio 98:2) was drop-casted and dried overnight at 4 °C.

pH sensor. The carbon electrode was initially cleaned using 0.5 M HCl by ten cyclic voltammetry cycles (−0.1 to 0.9 V) at a scan rate of 0.1 V s^{-1}. A PANI film was deposited in a 0.1 M aniline dissolved in 1 M HCl by applying 12 cyclic voltammetry cycles (−0.2 to 1 V) at a scan rate of 0.1 V s^{-1}. The same deposition procedure was repeated and dried overnight at 4 °C.

Reference electrode. A silver layer was deposited onto the AuNP electrode in a solution containing 250 mM silver nitrate, 750 mM sodium thiosulfate and 500 mM sodium bisulfite using multicurrent deposition (30 s at −1 µA, 30 s at −5 µA, 30 s at −10 µA, 30 s at −50 µA, 30 s at −0.1 mA and 30 s at −0.2 mA), followed by drop-casting 1 µl of 0.1 M $FeCl_3$ for 1 min. Then, 1 µl of PVB/NaCl solution containing 78.1 mg of PVB and 50 mg of NaCl in 1 ml of methanol was drop-casted onto the Ag/AgCl electrode and air dried overnight at 4 °C. For stabilization, the electrode was preconditioned in a solution containing 1 M KCl for 3 h before measurements[46].

Sensor dependency tests on pH, ionic strength and temperature. The dependency of the glucose and serotonin sensors on pH, ionic strength and temperature was evaluated under controlled conditions. For the glucose sensor, the amperometric response was measured by varying the pH from 5 to 8 in 1× SIF at room temperature, the ionic strength from 0.1× to 2× in SIF (pH 7.0) at room temperature and the temperature from 25 to 40 °C in 1× SIF (pH 7.0).

For the serotonin sensor, the ratiometric signal (*S*) was determined by measuring the voltammetry peak currents at 10 Hz and at a non-responsive frequency under various conditions. The measurements were conducted by varying the pH from 5.5 to 7.5 in 1× SIF at room temperature, the ionic strength from 0.1× to 2× in SIF (pH 7.0) and the temperature from 25 to 41 °C in SIF (pH 7.0).

To assess the dependency of each parameter for both sensors, a single parameter was varied while the other conditions were kept constant. The dependency of the ionic strength sensor on temperature was tested by varying the temperature from 25 to 45 °C in SIF (pH 7.0). The experimental data obtained for each condition were rendered and fitted to a fourth-order polynomial for quantitative analysis (Supplementary Figs. 23–26).

Preparation of SIF

The SIF contains 5.76 mM KCl, 1.44 mM KH_2PO_4, 115.4 mM NaCl, 8 mM Na_2HPO_4 and 0.33 mM $MgCl_2(H_2O)_6$ in deionized water. The pH was adjusted to 7.0 by adding HCl (ref. 47).

Preparation of sampled biofluids

Human faecal fluid. Human stool was collected from a healthy participant, strictly adhering to established ethical guidelines as delineated in protocols approved by the institutional review board at the California Institute of Technology (Caltech) (number IR24-0892) and mixed with deionized water at a 1:2 weight-to-volume ratio. This mixture was centrifuged for 30 min at 17,500*g*. The supernatant was collected and filtered using a spin column (Whatman Centrifuge Tube Filter 400 µl, polypropylene, 0.45 µm). The filtered samples were stored at −80 °C.

Rat intestinal fluid. Rat intestines were extracted from female Sprague Dawley rats after euthanasia and sectioned into five parts. The interior fluid was collected from each section and centrifuged for 10 min at 16,000*g* to filter out impurities and leftover material. The samples were stored at −80 °C.

Electronic system design and characterization

An electronic system was integrated into a highly compact four-layer PCB, with dimensions of 23 × 6.5 mm^2, crafted using Eagle CAD. The system's energy was harnessed from two series-connected silver oxide batteries (catalogue no. SR521SW; Energizer), delivering a combined voltage of 3.1 V with a capacity of 16 mAh. Power management within the system was diligently administered through a magnetic reed switch (catalogue no. MK24-B-3-OE; Standex-Meder Electronics) and a voltage regulator (catalogue no. ADP162; Analog Devices), ensuring consistent and stable power output. Wireless communication and control processes were managed by an adept radio frequency module (catalogue no. STM32WB1MMC; STMicroelectronics), responsible for wireless data transmission, signal processing and overseeing the electrochemical instrumentation system, which operated principally through the AD5940 (Analog Devices) and complemented by a voltage buffer (catalogue no. LPV521; Texas Instruments). The electronic system was proficient in continuous measurement operations, maintaining an average power consumption below 350 µW, thereby allowing for sustained operation for more than 20 h (Fig. 3d,e). A flowchart of the low-power device firmware, as well as the detailed breakdown of the system's power consumption is included in Supplementary Figs. 30 and 31 and Supplementary Table 5.

The power consumption of the electronic system was measured using a power profiler (catalogue no. PPK2; Nordic Semiconductor), and the dynamic power supply potentials during capsule device operation were recorded using a multiplexed electrochemical workstation (PalmSens 4; PalmSens).

To evaluate potential leakage, the PillTrek capsule was submerged in magnetically stirred rabbit intestinal fluid for 24 h (refs. 48,49). The weight was measured at 0, 5, 10, 15 and 24 h, remaining stable throughout (Supplementary Fig. 32a). After immersion, the operation of the capsule's electronic system was confirmed using a d.c. power supply (catalogue no. 2231A-30-3, Keithley Instruments), verifying that the capsule remained sealed and functional (Supplementary Fig. 32b,c).

Phantom intestine model in vitro experiment. A phantom intestine mould was designed and fabricated using 3D printing technology to simulate the GI environment. The mould was printed using

biocompatible polylactic acid material with dimensions replicating the average human intestinal tract. A capsule device was securely attached to a thin fishing line, which was then connected to a 12 V d.c. unipolar stepper motor through a 3D-printed reel (ELEGOO Mars 3; ELEGOO). The motor was controlled using a stepper motor driver (catalogue no. A4988, Allegro Microsystems) and an Arduino Uno, allowing precise control over the capsule's movement. The stepper motor was programmed to pull the capsule across the phantom model at a constant speed of 0.45 cm min^{-1}.

In vitro tissue collision experiment. The capsule device was suspended using a fishing line attached to an Arduino-controlled stepper motor (Supplementary Fig. 34). The fishing line was threaded through a hanger positioned above the tissue sample, allowing vertical movement of the capsule. Arduino firmware was developed to control the motor such that the capsule collided with and maintained contact with the animal tissue for 10 s during every 1-min cycle.

Data acquisition via user interfaces

Initially, data from the capsule sensor were collected using a BLE dongle (catalogue no. CY5677, Infineon Technologies). To enhance this system, we developed a custom mobile application (app) using the cross-platform Flutter framework (Fig. 3c). This app enables wireless communication with the wearable devices via BLE, allowing users to send commands and to acquire, process and visualize intestinal biomarker levels. It establishes a secure BLE connection to the capsule device. The home page features buttons for various user commands and displays the most recently measured analyte concentrations. The measurement page plots the converted and calibrated sensor responses in real time, illustrating the dynamic biochemical profile within the GI tract.

Cytocompatibility studies

The cytocompatibility of PillTrek was examined by culturing with human colorectal adenocarcinoma HT29 cells (ATCC, cultured under 37 °C and 5% CO_2). A commercial calcein AM–ethidium homodimer-1 live–dead kit (Invitrogen) was used to evaluate cell viability. A Zeiss confocal microscope was used for cell imaging. Presto blue staining (Invitrogen) was used for quantitative analysis of cell viability and a Biotek plate reader was used for optical density measurements.

Animal studies

Animal studies were conducted in vitro with a rat model to examine the influence of varying dietary intakes on GI biomarker levels and in vivo with a rabbit model to evaluate the performance of the fully integrated capsule device in a real intestinal environment. These study protocols were approved by the Institutional Animal Care and Use Committee (protocol nos. IA23-1800 for the rodent study and IA23-1865 for the rabbit study) at the California Institute of Technology.

In vitro rat diet studies. Healthy female Sprague Dawley rats, weighing between 200 and 300 g, were fasted for 12 h before replacing their water supply with more water, sugar-infused water (85.5 g of sugar in 250 ml of water) or a custom blended smoothie (20 g of sugar, one banana and 50 g of chia seeds in 250 ml of almond milk). After 2 h of feeding, the animals were euthanized, and the intestines were extracted for intestinal fluid collection. The collected fluids were analysed using the capsule sensor array. The serotonin content of the rat intestinal fluids was further analysed via ELISA.

In vivo rabbit studies. For in vivo evaluation of PillTrek, male *Oryctolagus cuniculus* rabbits, weighing between 3.6 and 4 kg, were fasted for 12 h before surgery. The rabbits were induced with ketamine (35 mg kg^{-1}, intramuscular) and xylazine (5 mg kg^{-1}, intramuscular), and with acepromazine (0.25–1 mg kg^{-1}, subcutaneous) used for fractious rabbits. Glycopyrrolate (0.1 mg kg^{-1}, subcutaneous) was administered to reduce salivary secretions, and ophthalmic ointment was applied to the corneas. An intravenous catheter was placed in the ear vein for blood sample collection. The rabbits were transitioned to a gas mask with isoflurane (1–5%) for continuous anaesthesia, positioned supine and monitored with a pulse oximeter and an electrocardiogram device. The surgical area was shaved, disinfected with 70% ethanol and anaesthetic depth was monitored by toe pinching, heart rate and respiratory rate.

Incisions were made along the midline at the linea alba using a blade. After opening the abdominal cavity, a 1–2 cm incision was made in the duodenum to insert the PillTrek and duodenostomy tube for administering PBS containing glucose or serotonin over several hours with a flow rate of 2 ml h^{-1}. The intestinal incision was sutured with 5-0 sterile sutures, and the abdominal incision was closed with 4-0 sterile sutures. An X-ray confirmed the capsule's location before and after data collection, and the rabbits remained under anaesthesia during imaging and testing. After an acclimatization time of 15 min, wireless data from the robotic capsules were transmitted to a laptop or smartphone. The stable baseline measurement of serotonin levels after a 15-min stabilization period postsurgery indicated the minimal influence of ketamine, xylazine and acepromazine in the serotonin dynamics during the study. Following the procedure, the duodenostomy tube was surgically removed, and another X-ray verified the capsule's position. After the studies and euthanasia, the capsule was retrieved surgically through the abdominal cavity.

Reporting summary

Further information on research design is available in Nature Portfolio Reporting Summary linked to this article.

Data availability

The data that supports the findings of this study are available from the corresponding authors on reasonable request. Source data are provided with this paper.

References

1. Steiger, C. et al. Ingestible electronics for diagnostics and therapy. *Nat. Rev. Mater.* **4**, 83–98 (2019).
2. Said, H. M. & Ghishan, F. K. (eds) *Physiology of the Gastrointestinal Tract* (Academic Press, 2018).
3. Dieterich, W., Schink, M. & Zopf, Y. Microbiota in the gastrointestinal tract. *Med. Sci.* **6**, 116 (2018).
4. McCallum, G. & Tropini, C. The gut microbiota and its biogeography. *Nat. Rev. Microbiol.* **22**, 105–118 (2024).
5. Smith, P. A. The tantalizing links between gut microbes and the brain. *Nature* **526**, 312–314 (2015).
6. Yano, J. M. et al. Indigenous bacteria from the gut microbiota regulate host serotonin biosynthesis. *Cell* **161**, 264–276 (2015).
7. Rea, K., Dinan, T. G. & Cryan, J. F. The microbiome: a key regulator of stress and neuroinflammation. *Neurobiol. Stress* **4**, 23–33 (2016).
8. Bhattacharyya, A., Chattopadhyay, R., Mitra, S. & Crowe, S. E. Oxidative stress: an essential factor in the pathogenesis of gastrointestinal mucosal diseases. *Physiol. Rev.* **94**, 329–354 (2014).
9. Vernia, P. et al. Fecal lactate and ulcerative colitis. *Gastroenterology* **95**, 1564–1568 (1988).
10. Mawe, G. M. & Hoffman, J. M. Serotonin signalling in the gut—functions, dysfunctions and therapeutic targets. *Nat. Rev. Gastroenterol. Hepatol.* **10**, 473–486 (2013).
11. Gershon, M. D. & Tack, J. The serotonin signaling system: from basic understanding to drug development for functional GI disorders. *Gastroenterology* **132**, 397–414 (2007).

12. Martin-Gallausiaux, C., Marinelli, L., Blottière, H. M., Larraufie, P. & Lapaque, N. SCFA: mechanisms and functional importance in the gut. *Proc. Nutr. Soc.* **80**, 37–49 (2021).
13. Dalile, B., Van Oudenhove, L., Vervliet, B. & Verbeke, K. The role of short-chain fatty acids in microbiota–gut–brain communication. *Nat. Rev. Gastroenterol. Hepatol.* **16**, 461–478 (2019).
14. Fallingborg, J. Intraluminal pH of the human gastrointestinal tract. *Dan. Med. Bull.* **46**, 183–196 (1999).
15. Press et al. Gastrointestinal pH profiles in patients with inflammatory bowel disease. *Aliment Pharmacol. Ther.* **12**, 673–678 (1998).
16. Chang, E. B. & Leung, P. S. in *The Gastrointestinal System* (ed. Leung, P. S.) 107–134 (Springer, 2014).
17. Maggs, D., MacDonald, I. & Nauck, M. A. Glucose homeostasis and the gastrointestinal tract: insights into the treatment of diabetes. *Diabetes Obes. Metab.* **10**, 18–33 (2008).
18. Fournel, A. et al. Glucosensing in the gastrointestinal tract: impact on glucose metabolism. *Am. J. Physiol. Gastrointest. Liver Physiol.* **310**, G645–G658 (2016).
19. Antunes, L. C. M., Davies, J. E. & Finlay, B. B. Chemical signaling in the gastrointestinal tract. *F1000 Biol. Rep.* **3**, 4 (2011).
20. Shalon, D. et al. Profiling the human intestinal environment under physiological conditions. *Nature* **617**, 581–591 (2023).
21. Kalantar-Zadeh, K., Ha, N., Ou, J. Z. & Berean, K. J. Ingestible sensors. *ACS Sens.* **2**, 468–483 (2017).
22. Cao, Q. et al. Robotic wireless capsule endoscopy: recent advances and upcoming technologies. *Nat. Commun.* **15**, 4597 (2024).
23. Nan, K. et al. Mucosa-interfacing electronics. *Nat. Rev. Mater.* **7**, 908–925 (2022).
24. Min, J., Yang, Y., Wu, Z. & Gao, W. Robotics in the gut. *Adv. Ther.* **3**, 1900125 (2020).
25. Abdigazy, A. et al. End-to-end design of ingestible electronics. *Nat. Electron.* **7**, 102–118 (2024).
26. Traverso, G. et al. First-in-human trial of an ingestible vitals-monitoring pill. *Device* **1**, 100125 (2023).
27. You, S. S. et al. An ingestible device for gastric electrophysiology. *Nat. Electron.* **7**, 497–508 (2024).
28. Kalantar-Zadeh, K. et al. A human pilot trial of ingestible electronic capsules capable of sensing different gases in the gut. *Nat. Electron.* **1**, 79–87 (2018).
29. Hou, B. et al. A swallowable X-ray dosimeter for the real-time monitoring of radiotherapy. *Nat. Biomed. Eng.* **7**, 1242–1251 (2023).
30. Inda-Webb, M. E. et al. Sub-1.4 cm^3 capsule for detecting labile inflammatory biomarkers in situ. *Nature* **620**, 386–392 (2023).
31. Mimee, M. et al. An ingestible bacterial-electronic system to monitor gastrointestinal health. *Science* **360**, 915–918 (2018).
32. De La Paz, E. et al. A self-powered ingestible wireless biosensing system for real-time in situ monitoring of gastrointestinal tract metabolites. *Nat. Commun.* **13**, 7405 (2022).
33. Xu, C. et al. A physicochemical-sensing electronic skin for stress response monitoring. *Nat. Electron.* **7**, 168–179 (2024).
34. Maines, A., Ashworth, D. & Vadgama, P. Diffusion restricting outer membranes for greatly extended linearity measurements with glucose oxidase enzyme electrodes. *Anal. Chim. Acta* **333**, 223–231 (1996).
35. Venton, B. J. & Cao, Q. Fundamentals of fast-scan cyclic voltammetry for dopamine detection. *Analyst* **145**, 1158–1168 (2020).
36. Li, J. et al. A tissue-like neurotransmitter sensor for the brain and gut. *Nature* **606**, 94–101 (2022).
37. Li, S. et al. A wrinkled structure of gold film greatly improves the signaling of electrochemical aptamer-based biosensors. *RSC Adv.* **11**, 671–677 (2020).
38. Li, H., Dauphin-Ducharme, P., Ortega, G. & Plaxco, K. W. Calibration-free electrochemical biosensors supporting accurate molecular measurements directly in undiluted whole blood. *J. Am. Chem. Soc.* **139**, 11207–11213 (2017).
39. Jang, H.-S. et al. Nafion coated Au nanoparticle-graphene quantum dot nanocomposite modified working electrode for voltammetric determination of dopamine. *Inorg. Chem. Commun.* **105**, 174–181 (2019).
40. Ren, J., Shi, W., Li, K. & Ma, Z. Ultrasensitive platinum nanocubes enhanced amperometric glucose biosensor based on chitosan and Nafion film. *Sens. Actuators B* **163**, 115–120 (2012).
41. David, L. A. et al. Diet rapidly and reproducibly alters the human gut microbiome. *Nature* **505**, 559–563 (2014).
42. Margolis, K. G. et al. Pharmacological reduction of mucosal but not neuronal serotonin opposes inflammation in mouse intestine. *Gut* **63**, 928–937 (2014).
43. Zelkas, L. et al. Serotonin-secreting enteroendocrine cells respond via diverse mechanisms to acute and chronic changes in glucose availability. *Nutr. Metab.* **12**, 55 (2015).
44. O'Mahony, S. M., Clarke, G., Borre, Y. E., Dinan, T. G. & Cryan, J. F. Serotonin, tryptophan metabolism and the brain-gut-microbiome axis. *Behav. Brain Res.* **277**, 32–48 (2015).
45. Nath, S. et al. Topographical and biometrical anatomy of the digestive tract of white New Zealand rabbit (*Oryctolagus cuniculus*). *J. Adv. Vet. Anim. Res.* **3**, 145–151 (2016).
46. Gao, W. et al. Fully integrated wearable sensor arrays for multiplexed in situ perspiration analysis. *Nature* **529**, 509–514 (2016).
47. Brodkorb, A. et al. INFOGEST static in vitro simulation of gastrointestinal food digestion. *Nat. Protoc.* **14**, 991–1014 (2019).
48. Del-Rio-Ruiz, R. et al. Soft autonomous ingestible device for sampling the small-intestinal microbiome. *Device* **2**, 100406 (2024).
49. Levy, J. A., Straker, M. A., Stine, J. M., Beardslee, L. A. & Ghodssi, R. Magnetically triggered ingestible capsule for localized microneedle drug delivery. *Device* **2**, 100438 (2024).

Acknowledgements

This project was supported by the National Science Foundation grant no. 2145802, National Institutes of Health grant nos. R01HL155815 and R21DK13266, American Cancer Society Research Scholar grant no. RSG-21-181-01-CTPS, Army Research Office grant no. W911NF-23-1-0041, US Army Medical Research Acquisition Activity grant no. HT9425-24-1-0249, National Research Foundation of Korea grant no. RS-2024-00411904 and Heritage Medical Research Institute (all to W.G.). We gratefully acknowledge critical support and infrastructure provided for this work by the Kavli Nanoscience Institute at Caltech. J.M. acknowledges fellowship support from the National Institutes of Health Training grant (no. T32EB023858). H.A. and H.-T.J. acknowledge the support from the KAIST-UC Berkeley-VNU Climate Change Research Center grant no. 2021K1A4A8A01079356. Lemberg (Austria) helped with porting code.

Author contributions

W.G. and J.M. initiated the concept of and designed the studies. W.G. supervised the work. J.M. and H.A. led the experiments and collected the overall data. H.L., R.B. and G.K. contributed to sensor characterization and validation. X.M., S.-H.S., C.W., Y.X. and D.R.Y contributed to the animal studies. Z.L., T.K.H., A.E. and H.-T.J. contributed to the study design. All authors contributed to the data analysis and provided the feedback on the paper.

Competing interests
The authors declare no competing interests.

Additional information
Supplementary information The online version contains supplementary material available at https://doi.org/10.1038/s41928-025-01407-0.

Correspondence and requests for materials should be addressed to Hee-Tae Jung or Wei Gao.

Peer review information *Nature Electronics* thanks Rabia Yazicigil and the other, anonymous, reviewer(s) for their contribution to the peer review of this work.

[1]Andrew and Peggy Cherng Department of Medical Engineering, Division of Engineering and Applied Science, California Institute of Technology, Pasadena, CA, USA. [2]Department of Chemical and Biomolecular Engineering, Korea Advanced Institute of Science and Technology, Daejeon, Republic of Korea. [3]Division of Clinical Nutrition, David Geffen School of Medicine, University of California, Los Angeles, CA, USA. [4]Division of Cardiology, Department of Medicine, David Geffen School of Medicine, University of California, Los Angeles, CA, USA. [5]Department of Electrical Engineering, Division of Engineering and Applied Science, California Institute of Technology, Pasadena, CA, USA. [6]These authors contributed equally: Jihong Min, Hyunah Ahn. ✉e-mail: heetae@kaist.ac.kr; weigao@caltech.edu

nature research

Corresponding author(s): Wei Gao

Last updated by author(s): 05/04/2025

Reporting Summary

Nature Research wishes to improve the reproducibility of the work that we publish. This form provides structure for consistency and transparency in reporting. For further information on Nature Research policies, see our Editorial Policies and the Editorial Policy Checklist.

Statistics

For all statistical analyses, confirm that the following items are present in the figure legend, table legend, main text, or Methods section.

n/a	Confirmed	
☐	☒	The exact sample size (*n*) for each experimental group/condition, given as a discrete number and unit of measurement
☐	☒	A statement on whether measurements were taken from distinct samples or whether the same sample was measured repeatedly
☐	☒	The statistical test(s) used AND whether they are one- or two-sided *Only common tests should be described solely by name; describe more complex techniques in the Methods section.*
☒	☐	A description of all covariates tested
☒	☐	A description of any assumptions or corrections, such as tests of normality and adjustment for multiple comparisons
☐	☒	A full description of the statistical parameters including central tendency (e.g. means) or other basic estimates (e.g. regression coefficient) AND variation (e.g. standard deviation) or associated estimates of uncertainty (e.g. confidence intervals)
☒	☐	For null hypothesis testing, the test statistic (e.g. *F*, *t*, *r*) with confidence intervals, effect sizes, degrees of freedom and *P* value noted *Give P values as exact values whenever suitable.*
☒	☐	For Bayesian analysis, information on the choice of priors and Markov chain Monte Carlo settings
☒	☐	For hierarchical and complex designs, identification of the appropriate level for tests and full reporting of outcomes
☒	☐	Estimates of effect sizes (e.g. Cohen's *d*, Pearson's *r*), indicating how they were calculated

Our web collection on statistics for biologists contains articles on many of the points above.

Software and code

Policy information about availability of computer code

Data collection	Presto blue staining (Invitrogen) was used for quantitative analysis of cell viability and Biotek plate reader was used for OD measurements. Zeiss confocal microscope was used for cell imaging. CH Instrument was used for sensor characterization.
Data analysis	Python 3.10.11 was used to analyze all data, plot the data and calculate the statistical parameters.

For manuscripts utilizing custom algorithms or software that are central to the research but not yet described in published literature, software must be made available to editors and reviewers. We strongly encourage code deposition in a community repository (e.g. GitHub). See the Nature Research guidelines for submitting code & software for further information.

Data

Policy information about availability of data

All manuscripts must include a data availability statement. This statement should provide the following information, where applicable:

- Accession codes, unique identifiers, or web links for publicly available datasets
- A list of figures that have associated raw data
- A description of any restrictions on data availability

The main data supporting the results in this study are available within the paper and its Supplementary Information. Source data are provided with this paper

Field-specific reporting

Please select the one below that is the best fit for your research. If you are not sure, read the appropriate sections before making your selection.

☒ Life sciences ☐ Behavioural & social sciences ☐ Ecological, evolutionary & environmental sciences

For a reference copy of the document with all sections, see nature.com/documents/nr-reporting-summary-flat.pdf

Life sciences study design

All studies must disclose on these points even when the disclosure is negative.

Sample size	For in vitro cell studies at least 3 samples per group per time point was tested (n≥3). For in vito rat studies 3 animals per condition was tested. For in vivo rabbit studies, two animals were tested. Sample size calculations were not formally performed for this exploratory study. Instead, sample sizes were determined based on established practices in similar proof-of-concept studies evaluating biocompatibility and device performance.
Data exclusions	No data exclusion.
Replication	All attempts at replication were successful when following the device fabrication process described in the paper.Device fabrication and functional testing were successfully reproduced across multiple batches, with all attempts at replication yielding consistent results when following the procedures described in the manuscript.
Randomization	The device was fabricated with same process and was tested in all animals under same conditions. Randomization was therefore not relevant to the study.
Blinding	Not relevant, because a blinding process wouldn't influence the sampling result.

Reporting for specific materials, systems and methods

We require information from authors about some types of materials, experimental systems and methods used in many studies. Here, indicate whether each material, system or method listed is relevant to your study. If you are not sure if a list item applies to your research, read the appropriate section before selecting a response.

Materials & experimental systems

n/a	Involved in the study
☒	☐ Antibodies
☐	☒ Eukaryotic cell lines
☒	☐ Palaeontology and archaeology
☐	☒ Animals and other organisms
☐	☒ Human research participants
☒	☐ Clinical data
☒	☐ Dual use research of concern

Methods

n/a	Involved in the study
☒	☐ ChIP-seq
☒	☐ Flow cytometry
☒	☐ MRI-based neuroimaging

Eukaryotic cell lines

Policy information about cell lines

Cell line source(s)	Human colorectal adenocarcinoma HT29 cells (ATCC, cultured under 37 °C and 5% CO2)
Authentication	All cells were purchased from ATCC and have been ethically sourced and authenticated by thorough QC testing by ATCC. No further in-lab authentication was conducted beyond routine morphological verification during culture.
Mycoplasma contamination	We did not observe any mycoplasma contamination in our cell cultures.
Commonly misidentified lines (See ICLAC register)	The cell culture experiment was conducted once, and quantitative analysis of cell viability was based on three independent image-based measurements from different representative fields of view per condition.

Animals and other organisms

Policy information about studies involving animals; ARRIVE guidelines recommended for reporting animal research

Laboratory animals	The animals used in this study included female Sprague Dawley rats (~8–10 weeks old, 200–300 g, Charles River Laboratories,

Laboratory animals	Wilmington, MA, USA) for in vitro diet studies and male Oryctolagus cuniculus rabbits (~4–6 months old, 3.6–4 kg, Charles River Laboratories, Wilmington, MA, USA) for in vivo capsule evaluation.
Wild animals	No field collected samples were used in the study.
Field-collected samples	No field collected samples were used in the study.
Ethics oversight	The animal protocol was approved by the Institutional Animal Care and Use Committee (IACUC) (Protocol No. IA20-1800 and IA23-1865) at California Institute of Technology.

Note that full information on the approval of the study protocol must also be provided in the manuscript.

Human research participants

Policy information about studies involving human research participants

Population characteristics	For human stool collection, a single healthy adult participant between the ages of 18 and 65 was recruited. The individual met general health criteria with no known gastrointestinal disorders or recent antibiotic use.
Recruitment	The healthy participant was recruited from Caltech campus, the neighboring communities through advertisement by posted notices, word of mouth, and email distribution. The participant gave written informed consent before participation in the study.
Ethics oversight	Institutional Review Board (IRB) at the California Institute of Technology

Note that full information on the approval of the study protocol must also be provided in the manuscript.